Available online at www.sciencedirect.com
ScienceDirect
Journal of Solid State Chemistry 180 (2007) 3039–3048
JOURNAL OF SOLID STATE CHEMISTRY
www.elsevier.com/locate/jssc

Novel perovskite-related barium tungstate $Ba_{11}W_4O_{23}$

Seung-Tae Hong*

LG Chem Research Park, Daejeon 305-380, South Korea

Received 19 June 2007; received in revised form 24 August 2007; accepted 26 August 2007
Available online 8 September 2007

Abstract

$Ba_{11}W_4O_{23}$ was synthesized at 1300 °C, followed by quenching with liquid nitrogen. The crystal structure, which was known to be cryolite-related but has remained unclear, was initially determined by single-crystal X-ray diffraction for the isostructural Ru-substituted compound $Ba_{11}(W_{3.1}Ru_{0.9})O_{22.5}$, which was discovered during exploratory synthesis in the Ba–Ru–O system. The structure of $Ba_{11}W_4O_{23}$ was refined by a combined powder X-ray and neutron Rietveld method (*Fd*-3*m*, $a = 17.1823(1)$ Å, $Z = 8$, $R_p = 3.09\%$, $R_{wp} = 4.25\%$, $\chi^2 = 2.8$, 23 °C). The structure is an example of *A*-site vacancy-ordered $4 \times 4 \times 4$ superstructure of a simple perovskite ABO_3, and it may be written as $(Ba_{1.75}\square_{0.25})BaWO_{5.75}\square_{0.25}$, emphasizing vacancies on both metal and anion sites. The local structure of one of two asymmetric tungsten ions is the WO_6 octahedron, typical of perovskite. The other tungsten, however, is surrounded by oxygen and anionic vacancies statistically distributed over three divided sites to form 18 partially occupied oxygen atoms (~30% on average), represented as $WO_{18/3}$. The *A*-site cation-vacancies are ordered at the *8a* ($\frac{1}{8}$, $\frac{1}{8}$, $\frac{1}{8}$) site in between adjoining $WO_{18/3}$ polyhedra which form 1-D arrangements along [110] and equivalent directions. *In situ* high-temperature XRD data have shown that the quenched $Ba_{11}W_4O_{23}$ at room temperature is isostructural to the high-temperature phase at 1100 °C.

Keywords: Barium tungsten oxide; Cation-vacancy ordering; Oxygen disordering; Perovskite-related structure; Metal-defect; Oxygen-defect

1. Introduction

The perovskite ABO_3 has been one of the most studied oxide compounds in solid-state chemistry. The structure can be described as a three-dimensional BO_6 network resulting from the corner sharing of BO_6 octahedra and the A atoms which occupy the large 12-fold coordinated cubo-octahedral cavities. Some of these materials have an ideal cubic structure while most are distorted [1]. A doubled superstructure is known for the composition of the type $AA'BB'O_6$, or in general for a multiple occupation of the A or B sublattices through cation ordering. B-cation ordering is more common than A-cation ordering [1,2]. The cryolite structure A_3BO_6 (named after the mineral Na_2NaAlF_6) is another example of double perovskites of the type A_2ABO_6. The vacancies in the cation-site or the oxygen-site can be ordered to form superstructures as well. *A*-site vacancy-orderings are found in compounds such as $Li_{0.18}La_{0.61}\square_{0.21}TiO_3$ [3], $Sr_{1-3x/2}La_x\square_{x/2}TiO_3$ [4], $(Ba_{7/4}\square_{1/4})BaOsO_6$ [5], $(Sr_{7/4}\square_{1/4})SrReO_6$ [6], or $(La_{4/3}\square_{2/3})MgWO_6$ [7]. Examples of *B*-site vacancy-ordered perovskites include $Ba_2(B_{3/4}\square_{1/4}Sb)O_6$ (B = Ce [8,9], Zr [10]), and many compounds with ordered oxygen-vacancies are also known [11].

Exploratory synthesis in the search for new compounds, structures, and properties leads to the discovery of new phases, sometimes unexpected or unforeseen. The compounds reported in the $BaO–WO_3$ system are $BaWO_4$ [12], $Ba_3W_2O_9$ [13], Ba_2WO_5 [14], Ba_3WO_6, and $Ba_{2.75}WO_{5.75}$. Structural determinations have been carried out for the first three of the compounds. Ba_3WO_3 was first reported in 1946 [15,16]. However, there are substantial discrepancies among the results of different authors concerning its crystal structure and polymorphic transformation [17–21]. According to the phase composition and X-ray diffraction study on $Ba_{3-x}WO_{6-x}$ ($x = 0.0–0.4$), the distinct cubic structure of off-stoichiometric $Ba_{2.75}WO_{5.75}$ from Ba_3WO_6 was first noticed by Balashov et al. [21], and was also implied by a previous study [20]. Although the cryolite

*Fax: +82 42 861 2057.
E-mail address: sthong@lgchem.com

0022-4596/$ - see front matter © 2007 Elsevier Inc. All rights reserved.
doi:10.1016/j.jssc.2007.08.027

structure was assumed for these phases, the detailed structural model for Ba_3WO_6 or $Ba_{2.75}WO_{5.75}$ ($Ba_{11}W_4O_{23}$) has so far remained unclear. Single crystals of the Ru-doped $Ba_{11}W_4O_{23}$ were discovered unexpectedly during the attempts to explore for new compounds in the Ba–W–Ru–O system, providing an initial motivation to study $Ba_{11}W_4O_{23}$. The present paper describes the synthesis and the novel crystal structure of cubic $Ba_{11}W_4O_{23}$. This would be the first example of a cubic $4 \times 4 \times 4$ superstructure of a perovskite-related phase due to ordered *A*-site metal vacancies and disordered oxygen and anionic vacancies, determined from single-crystal X-ray diffraction data for $Ba_{11}(W_{3.1}Ru_{0.9})O_{22.5}$ and combined powder X-ray and neutron diffraction data for $Ba_{11}W_4O_{23}$.

2. Experimental

2.1. Single-crystal discovery

Single crystals of Ru-doped $Ba_{11}W_4O_{23-y}$ ($y \sim 0.5$) were obtained from the reactants of high-purity $BaCO_3$ (Cerac, 99.99%), WO_3 (Cerac, 99.99%), and RuO_2 (Strem, 99.99%). These were mixed in a 3:1:1 Ba:W:Ru ratio, pressed into a pellet, heated at 1300 °C for 12 h, and again at 1350 °C for 12 h with intermittent grinding and pressing. The product, which showed some unidentified phases by XRD, was then mixed with a 10-fold excess of $BaCl_2 \cdot 2H_2O$ in an alumina crucible, heated to 1000 °C for 6 days, and cooled slowly to 840 °C at a rate of 0.08 °C/h, after which the furnace was turned off. Light brown single crystals formed on the top edge of the crucible. Several crystals were analyzed by electron microprobe, which revealed that the crystals were barium tungsten oxide containing a small amount of Ru ions with a Ru/(Ru + W) ratio in the range between 10% and 30%. The crystals were used for structural determination.

2.2. Powder synthesis of $Ba_{11}W_4O_{23}$

Once the structure and metal composition were determined from the single-crystal analysis, Ru-free $Ba_{11}W_4O_{23}$ was prepared from a mixture of high-purity $BaCO_3$ (Strem, 99.999%), and WO_3 (Acros, 99.995%) in the stoichiometric composition of 11:4. The weighted powder was mixed in an agate mortar and pestle, pressed into pellets and then placed in an alumina crucible. The crucible was first heated at 1000 °C for 24 h, and again at 1150 °C for 35 h with intermittent mixing and pressing. Finally, the pellets after remixing were heated at 1300 °C for 10 h, cooled to 1100 °C, and then quenched with liquid nitrogen. The heating and cooling rate was 200 °C/h for all steps except the quenching process. The final product was a cubic single phase as shown by the XRD pattern, and had a white color at room temperature. For comparison, some samples were slowly cooled in the final heat treatment. Powder XRD patterns of these samples showed a non-cubic and unidentified crystal system.

2.3. Single-crystal X-ray study

Laue photographs were used to check the suitability for intensity data collection of single crystals of $Ba_{11}(W_{4-x}Ru_x)O_{23-y}$. Cubic symmetry was first obtained during an automatic searching routine in an ordinary four-circle diffractometer, and precession photos were used later to confirm the symmetry and possible space groups. Diffraction data for $Ba_{11}(W_{3.1}Ru_{0.9})O_{22.5}$ were collected at room temperature on a single-crystal diffractometer (Rigaku AFC6R) with graphite-monochromatic Mo*K*α radiation over two octants of reciprocal space ($2\theta \leqslant 60°$) from a 0.10 mm × 0.12 mm × 0.13 mm crystal. The unit cell parameter 17.141(1) Å was obtained from a least-squares refinement with 20 automatically centered reflections between 30° and 35°. A total of 3896 reflections were collected. The extinction conditions suggested two possible cubic space groups of centric *Fd*-3*m* (no. 227) and acentric *Fd*-3 (no. 203), consistent with the film results. Though an $N(Z)$ test of intensity statistics suggested a centric space group, both space groups turned out later to give basically the same structural solution. Thus, the higher symmetry *Fd-3m* was chosen, which gave 393 unique data ($R_{int} = 7.8\%$). Absorption was first corrected with the aid of the average of three psi-scans (transmission range of 0.784–1.000). Direct method [22] was used for the solution of the structure, suggesting most metal positions. The remainder of the refinement [23] was entirely routine, except for the presence of oxygen atoms surrounding W2. The overall Ru/W ratio was estimated first from electron microprobe analysis. The occupancy sum of W and Ru for each site was constrained to be unity, and Ru/W for each site was least-squares refined. Because of the strong correlation between the occupancy and thermal parameters, a similarity restraint [23] on the thermal parameters of W1 and W2 was applied to the refinement so that U_{iso}'s for the two atom sites are similar within the e.s.d. of 0.01 Å^2. The residuals at this stage were $R_F/R_w = 5.3\%/6.0\%$ ($I > 3\sigma(I)$, 200 unique reflections) without any oxygen bonded to W2 after all the other atoms including O1 were anisotropically refined and the W/Ru ratios were refined. The observed and difference Fourier maps around W2 are shown in Fig. 1, indicating three split sites of oxygen atoms (O2, O3, and O4). Based on these maps, a model with statistically distributed oxygen atoms was proposed. The partial occupancies of those oxygen sites were refined with a constraint that would satisfy the charge neutrality condition of the compound. The final residuals after the complete anisotropic refinement, except for the disordered oxygens (O2, O3, and O4), were $R_F/R_w = 4.0/5.1\%$ (43 variables). The largest residual peak in the ΔF map was $+0.50\,e^-/Å^3$, ~0.4 Å from Ba2, and $-0.30\,e^-/Å^3$, ~2.6 Å from O2, respectively. The most negative hole was the metal vacancy site at *8a* ($\frac{1}{8}, \frac{1}{8}, \frac{1}{8}$). Data collection and refinement parameters are given in Table 1. The final atom parameters and isotropic temperature factors are given in Table 2.

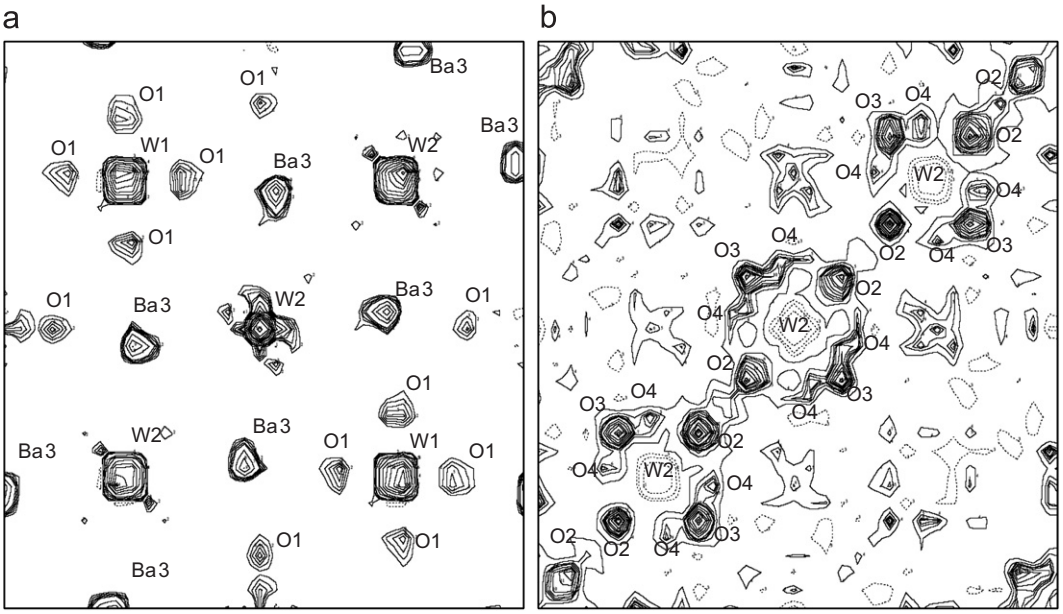

Fig. 1. (001) sections of (a) observed and (b) difference Fourier maps (XRD) at $z = 0$ for $Ba_{11}(W_{3.1}Ru_{0.9})O_{22.5}$ at the refinement stage prior to the location of O2, O3, and O4 atoms ($R_F/R_w = 5.3\%$, 6.0%). The map width is 16 Å, and the center of the map is the W2 position at (0,0,0). The dotted lines denote negative densities. The contour levels are adjusted unequally so that both the light and heavy atoms can be shown. The minimum and maximum contour levels are (a) −4 and ~74 e/Å^3, (b) −2.7 and 3.2 e/Å^3.

Table 1
Crystal data and structure refinement for single crystal $Ba_{11}(W_{3.1}Ru_{0.9})O_{22.5}$

Formula	$Ba_{11}W_{3.06(10)}Ru_{0.94(10)}O_{22.5(3)}$
Crystal color	Light brown
Formula weight	2528.0
Crystal system, space group, Z	Cubic, *Fd*-3*m* (no. 227), 8
Lattice constants (Å), V (Å^3)[a]	$a = 17.141(1)$, $V = 5036.3(5)$
d_{calc} (g/cm^3)	6.67
Crystal size (mm)	$0.10 \times 0.12 \times 0.13$
μ (Mo$K\alpha$, cm^{-1})	314.0
Radiation	Mo$K\alpha$ ($\lambda = 0.71069$ Å), graphite monochromated
Diffractometer	Rigaku AFC6R
Scan type	ω–2θ
Octants measured, $2\theta_{max}$	h, k, $\pm l$, 60°
Measured reflections	3896
Independent reflections	393
Observed reflections $F > 3\sigma(F)$	200
t (K)	296
R_{int} (%)	7.8
Number of variables	43
Absorption corrections	Empirical, 3Ψ-scans
Trans. coefficient range	0.784–1.0 (Ψ-scans)
Secondary extinction coefficient[b]	12(2)
Goodness-of-fit	1.4
Largest residual peak (e/Å^3)	+0.5 e$^-$/Å^3, ~0.4 Å from Ba2, −0.63 e$^-$/Å^3, ~2.6 Å from O2
R_F, R_w[c]	4.0%, 5.1%

[a]Least-squared refinement of 20 reflections in the range of 30° and 35° (2θ) on the diffractometer at 23 °C.

[b]Larson's extinction parameter, r^* (Eq. (22) in A.C. Larson, in: F.R. Ahmed (Ed.), Crystallographic Computing, Munksgaard, Copenhagen, 1970, pp. 291–294).

[c]$R_F = \sum||F_o|-|F_c||/\sum|F_o|$; $R_w = [\sum w(|F_o|-|F_c|)^2/\sum w(F_o)^2]^{1/2}$; $w = 1/\sigma_F^2$.

2.4. Powder X-ray and neutron study

The powder X-ray diffraction data for $Ba_{11}W_4O_{23}$ were collected at room temperature on a Bragg-Brentano diffractometer (Bruker-AXS D8 Advance) with a Cu X-ray tube, focusing primary Ge(1 1 1) monochromator ($\lambda = 1.5405$ Å) and a Vantec position sensitive detector with a detector slit of 6° over an angular range of $5° \leqslant 2\theta \leqslant 151°$ at increments of 0.016662° and a total measurement time of 5 h. All the peaks were indexed with a face-centered cubic cell with $a = 17.1823(2)$ Å. Neutron powder diffraction measurements were performed using HANARO HRPD equipment with a 32 He-3 Multi-detector system and a Ge(3 3 1) monochromator, at the Korea Atomic Energy Research Institute, Daejeon, Korea. The data were collected with a wavelength of 1.8371 Å over the 2θ range of 9–159° at increments of 0.05° and a total measurement time of 3 h. The sample amount used was 13.1 g. The profile refinement computer program GSAS [24] was used for the calculation. Combined refinement of X-ray and neutron data for $Ba_{11}W_4O_{23}$ was performed with starting structural parameters from the single crystal results for $Ba_{11}(W_{3.1}Ru_{0.9})O_{22.5}$. In order to check and confirm the oxide ions (O2, O3, and O4), they were excluded at the beginning stage. X-ray data fit relatively well even without these oxygens, while the neutron data did not fit well. However, the oxygen ions were easily located by difference Fourier maps of neutron data, consistent with the single-crystal data. The partial occupancies of these ions were refined with the constraint to achieve a charge

Table 2
Atomic coordinates, site occupancies and isotropic displacement ($Å^2 \times 10^2$) for single-crystal $Ba_{11}(W_{3.1}Ru_{0.9})O_{22.5}$ at room temperature (SG = *Fd*-3*m*, no. 227, $a = 17.141(1)$ Å)

Atom	Site	*x*	*y*	*z*	Occupancy	U_{iso}[a] ($\times 100$)
Ba1	8*b*	0.375	0.375	0.375	1	2.4(2)
Ba2	48*f*	0.40158(18)	0.125	0.125	1	3.5(1)
Ba3	32*e*	0.22672(14)	0.22672(14)	0.22672(14)	1	4.9(1)
W1/Ru1[b]	16*d*	0.5	0.5	0.5	0.67(3)/0.33(3)	1.3(1)
W2/Ru2	16*c*	0	0	0	0.86(2)/0.14(2)	2.2(1)
O1	96*g*	0.4989(8)	0.4989(8)	0.6141(11)	1	2.9(4)
O2	96*g*	0.076(2)	0.076(2)	−0.013(3)	0.350(8)[c]	2.0(6)
O3	96*h*	0	0.074(3)	−0.074(3)	0.263(8)[c]	1.9(6)
O4	96*g*	0.015(3)	0.015(3)	−0.101(4)	0.264(8)[c]	1.7(6)

[a] $U_{iso} = (U_{11} + U_{22} + U_{33})/3$ for Ba, W/Ru and O1; O2, O3, and O4 were refined isotropically.
[b] The sum of the W and Ru occupancies for each site was constrained to be unity.
[c] The partial occupancies of O2, O3, and O4 were refined with a constraint that would satisfy the charge neutrality condition of the compound.

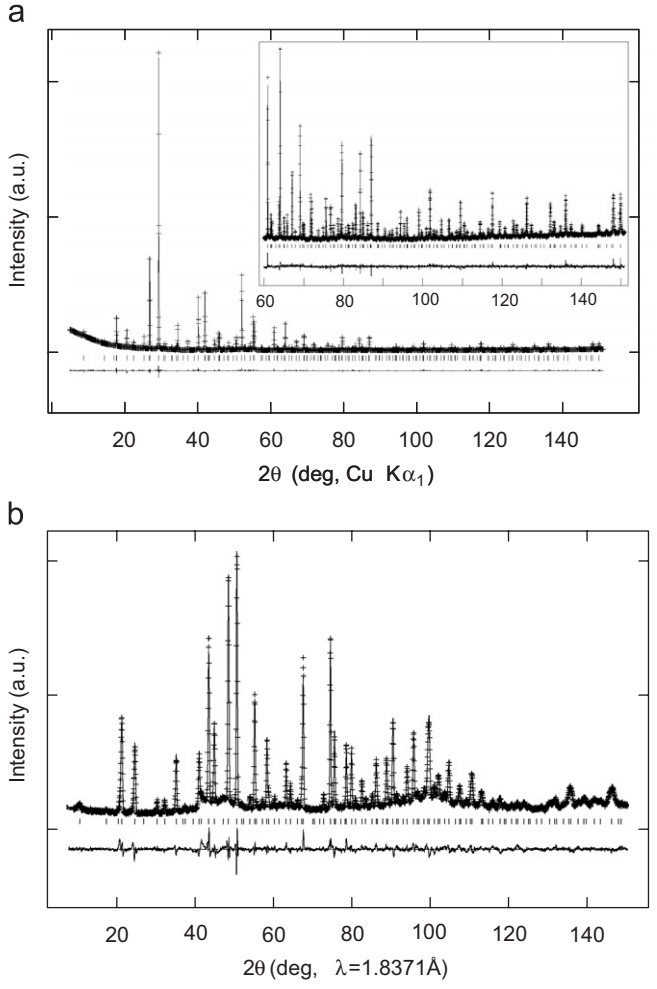

Fig. 2. Combined (a) X-ray ($\lambda = 1.5405$ Å) and (b) neutron ($\lambda = 1.8371$ Å) Rietveld refinement profiles for $Ba_{11}W_4O_{23}$, recorded at room temperature. The cross line marks experimental points and the solid line is the calculated profile. The lower trace shows the difference curve, and the ticks denote expected peak positions. The inset shows the high angle data in detail.

balance. Only the metal ions were anisotropically refined. A total of 103 parameters were refined including 25 structural parameters (cell parameter, 9 atomic coordinates, occupancies for O2, O3, and O4, and 2 isotropic and 10 anisotropic thermal parameters). The final residuals were $R_p/R_{wp} = 2.70\%/3.65\%$ for X-ray data, 4.70%/6.15% for neutron data, and 3.09%/4.25% in total with a χ^2 of 2.80. The final profile fits are shown in Fig. 2, and powder refinement results are given in Table 3. The refined atom parameters and isotropic temperature factors are given in Table 4, and the important bond distances and angles are given in Table 5. *In situ* high-temperature X-ray diffraction experiments as shown in Fig. 3 were performed at 25, 200, 400, 600, 800, 900, 1000, and 1100 °C using an Anton Paar HTK 1200 attached to the powder diffractometer described previously. Fig. 3 does not show all data for clarity. XRD data for Rietveld refinement were collected at 1100 °C after a waiting time for equilibrium of 13 h in the range of $8.5° \leqslant 2\theta \leqslant 151°$. However, data below 16° were excluded in the refinement because of the presence of broad background peaks coming from the high-temperature chamber itself around 14.5°. Rietveld refinement profiles for $Ba_{11}W_4O_{23}$ at 1100 °C are shown in Fig. 4, and the results are given in Table 6. Further details of the crystal structure investigations can be obtained from

Table 3
Crystal data and structure refinement for $Ba_{11}W_4O_{23}$ from combined powder X-ray and neutron diffraction data

Chemical formula	$Ba_{11}W_4O_{23}$
Formula weight	2614.1
Crystal system, space group, *Z*	*Fd*-3*m*, 8 (no. 227)
Lattice constants (Å), *V* ($Å^3$)	17.1823(2), 5072.8(2)
d_{calc} (g/cm^3)	6.84
Temperature (K)	296
Number of reflections (X-ray/neutron)	291/187
$R_p/R_{wp}/R_{exp}/R_B$ (X-ray) (%)[a]	2.70/3.66/2.47/6.04
$R_p/R_{wp}/R_{exp}/R_B$ (neutron) (%)[a]	4.71/6.17/2.97/7.80
R_p/R_{wp} (total) (%)[a]	3.09/4.26
Goodness-of-fit (total)	1.67
Reduced χ^2	2.80
Total refined parameters	103

[a] $R_p = 100\sum|I_o - I_c|/\sum|I_o|$; $R_{wp} = 100(\sum w|I_o - I_c|^2/\sum w|I_o|^2)^{1/2}$; $\chi^2 = 100\sum w|I_o - I_c|^2/(N_{obs} - N_{var})$; $R_{exp} = R_{wp}/|\chi|$.

Table 4
Atomic coordinates, site occupancies and isotropic displacement ($Å^2 \times 10^2$) for $Ba_{11}W_4O_{23}$ at room temperature (SG = *Fd*-3*m*, no. 227, $a = 17.1823(2)$ Å)

Atom	Site	*x*	*y*	*z*	Occupancy	U_{iso}[a]
Ba1	8*b*	0.375	0.375	0.375	1	2.41(8)
Ba2	48*f*	0.40000(5)	0.125	0.125	1	3.48(5)
Ba3	32*e*	0.22521(4)	0.22521(4)	0.22521(4)	1	4.83(5)
W1	16*d*	0.5	0.5	0.5	1	0.92(3)
W2	16*c*	0	0	0	1	1.76(3)
O1	96*g*	0.4998(1)	0.4998(1)	0.6124(1)	1	2.82(4)
O2	96*g*	0.0787(3)	0.0787(3)	−0.0054(4)	0.408(5)[b]	8.0(1)[c]
O3	96*h*	0	0.0791(4)	−0.0791(4)	0.310(10)[b]	8.0(1)[c]
O4	96*g*	0.0079(6)	0.0079(6)	−0.1104(7)	0.204(10)[b]	8.0(1)[c]

[a] $U_{iso} = (U_{11} + U_{22} + U_{33})/3$.
[b] The partial occupancies of O2, O3, and O4 were refined with a restraint that would satisfy the charge neutrality condition of the compound.
[c] Isotropic temperature factors of O2, O3, and O4 were constrained to be the same.

Table 5
Selected interatomic distances (Å) and angles (deg) in $Ba_{11}W_4O_{23}$ at room temperature

Ba1–O1 × 12	3.0496(19)	O1–W1–O1	180.0
Ba2–O1 × 4	2.7595(6)		89.82(8)
Ba2–O1 × 2	3.0405(19)		90.18(8)
Ba2–O2 × 2	2.727(6)		
Ba2–O3 × 4	2.592(5)	O4–W2–O4	180.0
Ba2–O4 × 2	2.926(14)		98.0(5)
Ba2–O4 × 4	3.3525(12)		82.0(5)
Ba3–O1 × 3	2.8544(16)	O4–W2–O2	131.0(3)
Ba3–O2 × 6	2.732(3)		98.6(4)
Ba3–O3 × 6	3.1097(14)		81.4(4)
Ba3–O4 × 3	2.126(12)		49.0(3)
		O4–W2–O3	138.9(3)
W1–O1 × 6	1.9305(14)		90.0
W2–O2 × 6	1.915(5)		41.1(3)
W2–O3 × 6	1.922(9)	O2–W2–O2	180.0
W2–O4 × 6	1.907(11)		115.5(3)
			64.5(3)
O2–O2 × 2	2.045(10)	O2–W2–O3	90.0
O2–O3 × 2	1.852(7)		122.3(2)
O2–O4 × 4	1.585(12)		57.7(2)
O3–O3 × 2	1.922(9)	O3–W2–O3	180.0
O3–O4 × 2	1.344(9)		120.0
			60.0

the Fachinformationszentrum Karlsruhe, 76344 Eggenstein-Leopoldshafen, Germany (fax: +49 7247 808 666; e-mail: crysdata@fiz-karlsruhe.de) on quoting the depository number CSD 418208 for single-crystal $Ba_{11}(W_{3.1}Ru_{0.9})O_{22.5}$, CSD 418207 for powder $Ba_{11}W_4O_{23}$, and CSD 418209 for powder $Ba_{11}W_4O_{23}$ at 1100 °C.

3. Results and discussion

3.1. Single-crystal study of $Ba_{11}(W_{3.1}Ru_{0.9})O_{22.5}$

The crystal structure solved using the direct method followed by routine refinement procedures resulted in a perovskite-related or cryolite-related structure with *A*-site metal-vacancy ordering. At the early stage of refinement, in the observed map as shown in Fig. 1a, the octahedrally coordinating oxygens (O1) around W1 were well located,

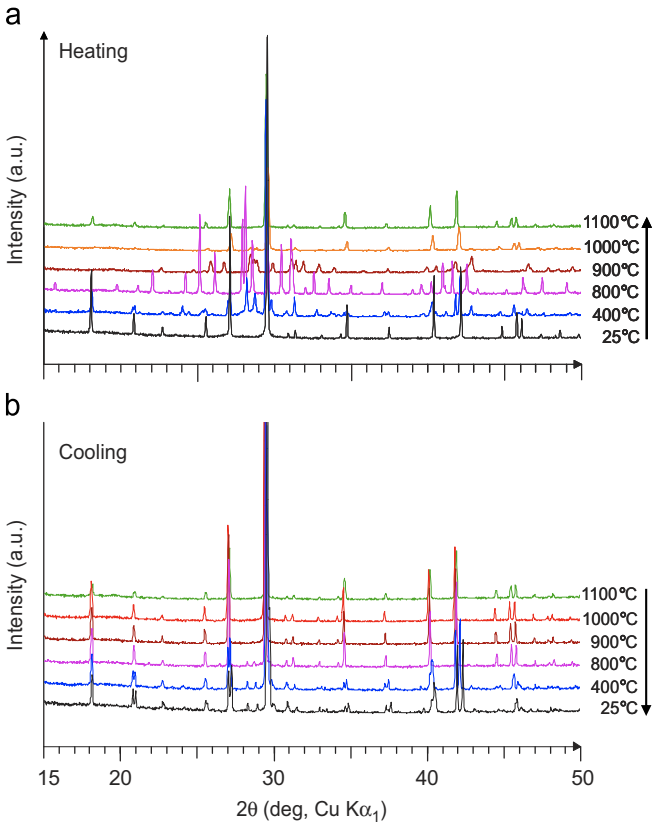

Fig. 3. *In situ* high-temperature X-ray diffraction patterns for $Ba_{11}W_4O_{23}$ that was quenched to liquid nitrogen from 1100 °C: (a) heating and (b) cooling.

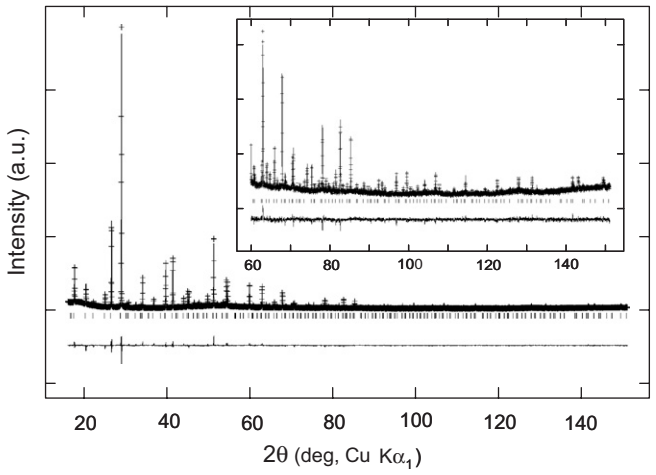

Fig. 4. X-ray ($\lambda = 1.5405$ Å) Rietveld refinement profiles for $Ba_{11}W_4O_{23}$, recorded at 1100 °C. The cross line marks experimental points and the solid line is the calculated profile. The lower trace shows the difference curve, and the ticks denote expected peak positions. The inset shows the high angle data in detail.

Table 6
Atomic coordinates, site occupancies and isotropic displacement ($Å^2 \times 10^2$) for $Ba_{11}W_4O_{23}$ at 1100 °C

Atom	Site	x	y	z	Occupancy	U_{iso}
Ba1	8*b*	0.375	0.375	0.375	1	6.2(2)
Ba2	48*f*	0.39938(10)	0.125	0.125	1	5.9(1)
Ba3	32*e*	0.22638(9)	0.22638(9)	0.22638(9)	1	11.0(1)
W1	16*d*	0.5	0.5	0.5	1	3.5(1)
W2	16*c*	0	0	0	1	4.1(1)
O1	96*g*	0.4936(5)	0.4936(5)	0.6150(4)	1	3.9(3)
O2[a]	96*g*	0.0787	0.0787	−0.0054	0.408	14(1)[b]
O3[a]	96*h*	0	0.0791	−0.0791	0.310	14(1)[b]
O4[a]	96*g*	0.0079	0.0079	−0.1104	0.204	14(1)[b]

SG = *Fd*-3*m*, no. 227, $Z = 8$; $a = 17.4966(2)$ Å; $V = 5356.3(2)$ Å^3; w$R_p = 6.74\%$, $R_p = 5.19\%$, $R_{exp} = 4.54\%$, $R_B = 11.6\%$; $\chi^2 = 2.2$.
[a]The values of O2, O3, and O4 positions and occupancies were from room temperature results.
[b]Isotropic temperature factors of O2, O3, and O4 were constrained to be the same.

but no clear atomic density was seen around W2. Non-octahedral electron densities around W2 were weak, but were observed in the difference Fourier map as shown in Fig. 1b. The total number of oxygen positions around W2 is 18, 3 of which are asymmetric (O2, O3, and O4) and are too close to each other to be occupied simultaneously. Because of the suspect coordination that could come from incorrect symmetry, possible lower symmetries were considered. For cubic *Fd*-3 (no. 203), tetragonal $I4_1/amd$ (no. 141), and trigonal *R*-3*m* (no. 166), which are maximal non-isomorphic subgroups of *Fd*-3*m* (no. 227), similar oxygen densities were found around the corresponding W2. Neither a more sensible model nor better refinement results were obtained. Thus, it was concluded that these disordered oxygens could indeed be a characteristic of the compound, not just a crystallographic misinterpretation.

The formal oxidation state of Ru was not confirmed experimentally, which would, by the charge neutrality condition, determine the oxygen content from 22.1 (for Ru^{4+}) to 22.5 (for Ru^{5+}) in $Ba_{11}(W_{3.1}Ru_{0.9})O_{23-y}$. However, assumptions of either Ru^{4+} or Ru^{5+} did not make any significant difference in the refinement results. Even though the higher oxidation Ru^{5+} was presumed for the refinement, giving a chemical formula of $Ba_{11}(W_{3.1}Ru_{0.9})O_{22.5}$, one cannot exclude a possibility of Ru^{4+} or a mixed state in the compound.

Structural investigation suggested later that $Ba_{11}(W_{3.1}Ru_{0.9})O_{22.5}$ (single crystal) and $Ba_{11}W_4O_{23}$ (powder) are isostructural. Neutron scattering data would be very helpful to determine and confirm the positions of the disordered oxygens of interest because neutron scattering length for oxygen atom is comparable with those for Ba or W. However, the neutron data were available only for the powder $Ba_{11}W_4O_{23}$, not for the single crystal of $Ba_{11}(W_{3.1}Ru_{0.9})O_{22.5}$. Thus, only the crystal structure of $Ba_{11}W_4O_{23}$ will be described in order to avoid repetition.

3.2. Phase stability

During synthesis, it was observed that the slow cooling of $Ba_{11}W_4O_{23}$ always resulted in a non-cubic phase with an unidentified crystal system. In order to confirm the stability region of the cubic phase, an *in situ* high-temperature XRD study was performed as shown in Fig. 3. Upon heating, the quenched cubic phase transformed to other phases. At 200 °C, only a small change was observed, as some single peaks started to split. Dramatic changes, new peaks for new phases, were observed between 400 and 900 °C, indicating that the quenched phase is quite unstable when heated. The cubic phase was recovered at 1100 °C. The precise recovering temperature was not determined in this investigation, but several different synthesis experiments demonstrated that the cubic phase could be obtained by quenching when it was heated above 1000 °C. Stepwise cooling resulted in less change, only showing a distortion from the cubic structure (Fig. 3b). More work is being undertaken to characterize the intermediate and slow cooled phases that will not be discussed in this paper.

3.3. Superstructure

The cubic cryolite A_3BO_6 structure with a unit cell dimension of $\sim 2a_p$ can be regarded as a $2 \times 2 \times 2$ superstructure of simple cubic perovskite ABO_3 with a_p. The off-stoichiometric $Ba_{2.75}WO_{5.75}$ (or $Ba_{11}W_4O_{23}$) from Ba_3WO_6 has $\sim 4a_p$. In the present study, even before determining the problematic oxygen positions, the metal positions determined in the early stage of refinement suggested the composition as either $(Ba_{2.75}\square_{0.25})WO_{5.75}\square_{0.25}$ or $(Ba_{1.75}\square_{0.25})BaWO_{5.75}\square_{0.25}$. The latter emphasizes the relationship with the double perovskite, $AA'BB'O_6$. The oxygen content of 5.75 was computed by the charge balance of the compound. The structure may be regarded as a cation-vacancy-ordered cryolite or double perovskite structure, forming a novel superstructure. Ba1 and Ba2 in Tables 2 and 4 correspond to *A*-site cations, while Ba3 and W correspond to *B*-site cations. It is interesting to note that similar compounds such as $Ba_2(B_{3/4}\square_{1/4}Sb)O_6$ (B = Ce [8,9], Zr [10]), $Ba_2(Ca_{1/4}Y_{3/4}\square_{1/4}U)O_6$ [25], $Ba_2(Ba_{7/8}\square_{1/8}U)O_{5.875}$ [26], and $Ba_2(Ba_{13/16}B_{2/16}\square_{1/16}U)O_6$ [27], are known to be *B*-site vacancy-ordered, while the present compound $(Ba_{7/4}\square_{1/4})BaWO_{5.75}$ is *A*-site vacancy-ordered with a cubic $4 \times 4 \times 4$ superstructure of a simple perovskite. It is similar in composition but different from other *A*-site vacancy-ordered perovskites with a tetragonal $2\sqrt{2} \times 2\sqrt{2} \times 4$ type superstructure as in $(Ba_{7/4}\square_{1/4})BaOsO_6$ [5] or $(Sr_{7/4}\square_{1/4})SrReO_6$ [6], or an orthorhombic $2 \times 4 \times 2$ type structure as in $(La_{4/3}\square_{2/3})MgWO_6$ [7].

3.4. Oxygen disordering

It was difficult to refine and confirm the structure using only with the powder X-ray data because of the weak scattering from the partially occupied oxygen atoms. The

neutron scattering data for $Ba_{11}W_4O_{23}$, however, provided quite clear results, and the oxygen positions were readily defined. Fig. 5 shows the (0 0 1) section of the Fourier synthesis map of neutron scattering density at $z = 0$ for $Ba_{11}W_4O_{23}$. The octahedral oxygen (O1) around W1 was well located with an almost equal density to W1, as expected from the similar neutron scattering lengths of W and O, whereas the oxygens O2, O3, and O4 around W2 have weaker but still clear densities. These are similar to the densities from the single crystal of $Ba_{11}(W_{3.1}Ru_{0.9})O_{22.5}$ shown in Fig. 1b. The weak densities coincide with the partial occupancies of the statistically distributed oxygens.

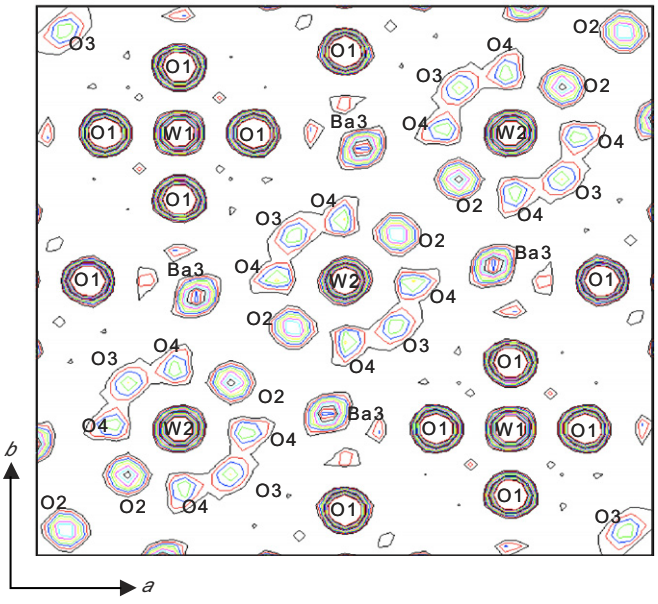

Fig. 5. (001) section of the Fourier synthesis map of neutron scattering density at $z = 0$ for $Ba_{11}W_4O_{23}$. The map width is 16 Å, and the center of the map is W2 at (0,0,0). The contour levels are adjusted so that weaker densities can be seen clearly.

Oxygen disorder or delocalization is uncommon, but is observed in some double perovskites such as Pb_2CoWO_6 [28] and Pb_2MgWO_6 [29], where the *B*-site cation is surrounded by 24 or 48 oxygens, respectively. Such anionic delocalization is also observed in fluorite structure as in the fast oxide ion conductor δ-Bi_2O_3 [30]. Fast Ag^+ cation conductors as in α-AgI or β-Ag_2S shows cation delocalization [31].

Fig. 6 shows the unit cell structure of $Ba_{11}W_4O_{23}$, where $W^{(1)}O_6$ is shown as a hatched one. The W2 environment may be represented as a $W^{(2)}O_{18/3}$ polyhedron to emphasize the total number of atoms (18) and the number of asymmetric sites (3) surrounding W2. In reality, the coordination polyhedron in $W^{(2)}O_{18/3}$ would, on a local scale, be one of the typical polyhedra observed in oxides. Fig. 7 displays a simple model where the $W^{(2)}O_{18/3}$ polyhedron on the left can be decomposed into the octahedron and four tetrahedra shown on the right, although other polyhedral coordinations such as square pyramidal WO_5 cannot be excluded.

The distinct environments around W1 and W2 are also of great interest (see Fig. 8). W1 has a typical perovskite *B*-site local environment. The nearest *A*-site cations are eight barium cations (two Ba1 and six Ba2) occupying the vertices of a slightly distorted cube. The distances of d(W1–Ba1) and d(W1–Ba2) are 3.720 and 3.490 Å, respectively. The distances between W1 and O1 and between O1 and the neighboring *B*-site atom (Ba3) are 1.931 and 2.854 Å, respectively, as expected from their ionic radii sums [32]. On the other hand, the other *B*-site atom W2 has shorter distances to oxygens: 1.915, 1.922,

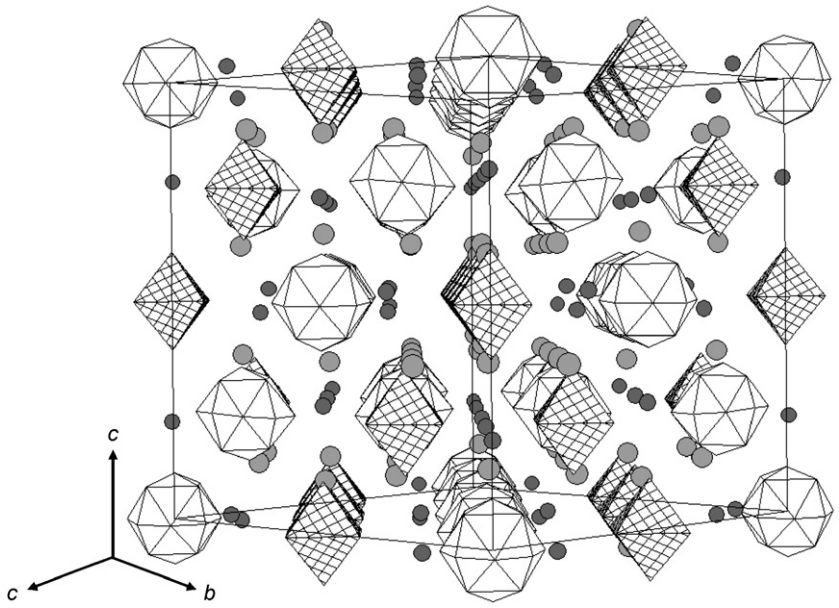

Fig. 6. (110) view of the crystal structure of $Ba_{11}W_4O_{23}$. $W^{(1)}O_6$ are shown as hatched octahedra, and $W^{(2)}O_{18/3}$ are shown as white polyhedra. Ba1 and Ba2 are shown as gray spheres, and Ba3 is represented as smaller darker spheres. The unit cell is outlined.

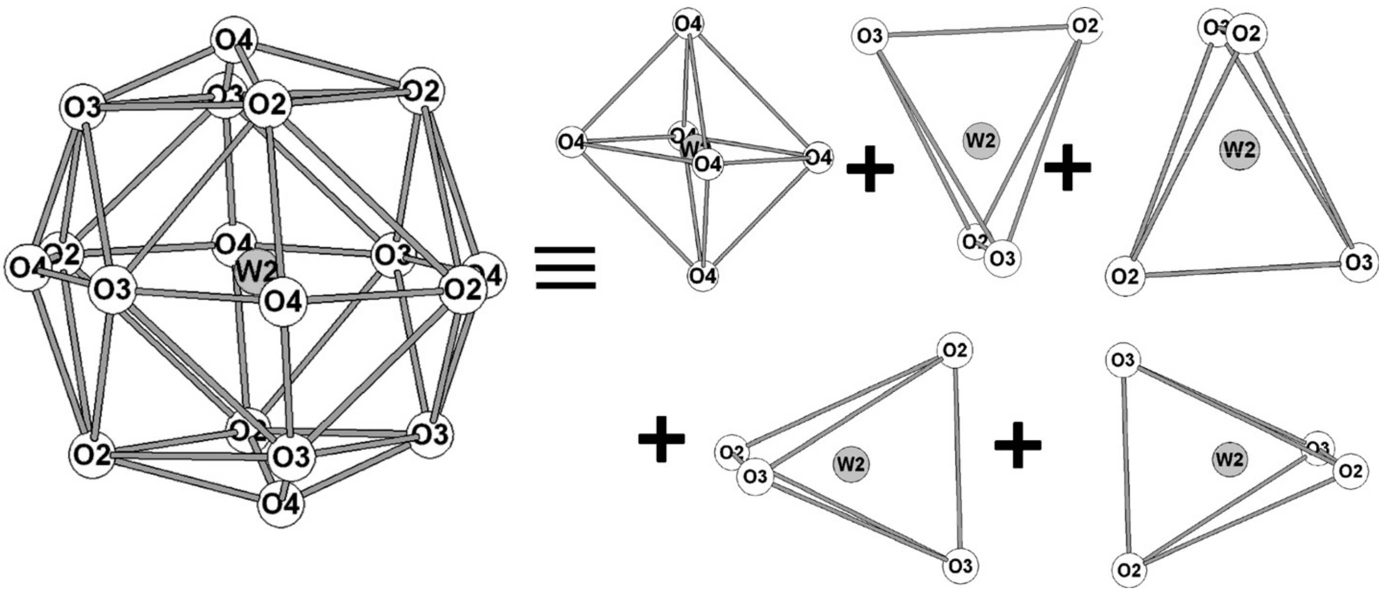

Fig. 7. Details of the $W^{(2)}O_{18/3}$ polyhedron are on the left, and a simple model is shown on the right, where it is decomposed into an octahedron and four tetrahedral. Oxide ions on $WO_{18/3}$ are statistically distributed over three sites (O2, O3, O4) with occupancies of ~30% on average.

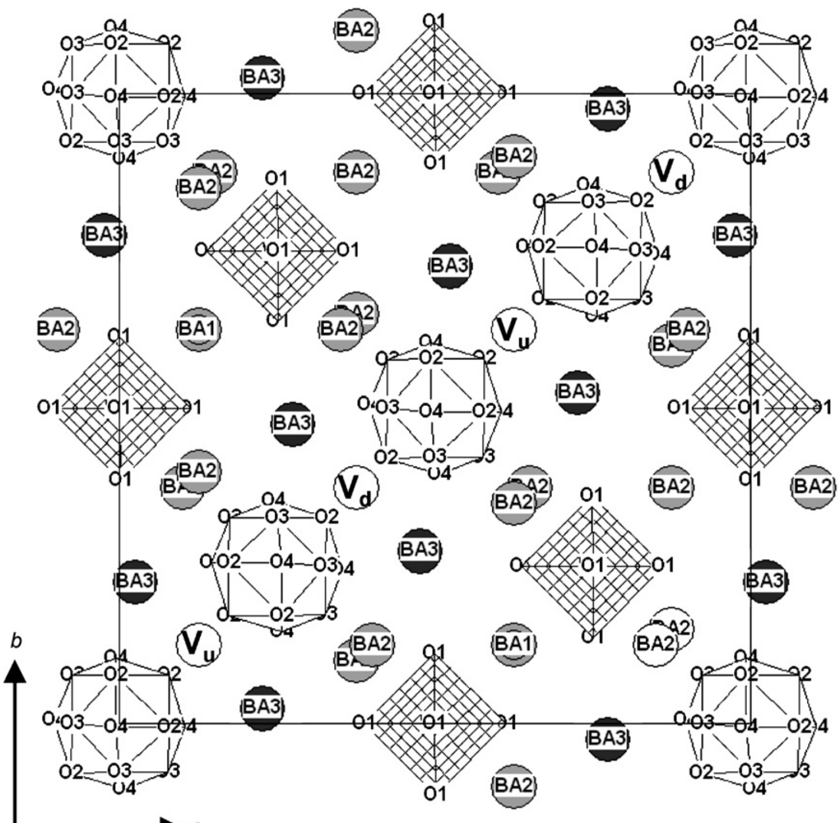

Fig. 8. A slab of the (001) plane around $z = 0$ with a thickness of ~5.0 Å for $Ba_{11}W_4O_{23}$. $W^{(1)}O_6$ is shown as a hatched octahedron. The lower left corner of the map is W2 at (0, 0, 0). Ba-vacancy sites are denoted as V_u and V_d, located above (at $z = 0.125$) and below (at $z = -0.125$) the slab, respectively. Ba-vacancies are ordered in between adjoining $W^{(2)}O_{18/3}$ polyhedra.

and 1.907 Å for O2, O3, and O4, respectively. W2 also has different nearest-metal surroundings. It has 12 Ba cations with similar distances: 6 *A*-site Ba2 and 6 *B*-site Ba3. Because of the *A*-site vacancy, only six *A*-site cations are surrounded instead of eight, but the distance from W2 to the *A*-site Ba2, 3.984 Å, is much longer than those for W1

(3.720 or 3.490 Å). More interestingly, the distance from W2 to the nearest *B*-site metal (Ba3), 3.916 Å, is shorter than the distance to the *A*-site (Ba2), exhibiting a strong distortion of the local structure around W2. O4 lies in midway between the two *B*-site metals of W2 and Ba3, resulting in a very short Ba3–O4 distance of 2.13 Å. This makes the O4 position unstable, consistent with the smallest occupancy factor of 0.204. There are some reported examples showing such short Ba–O distances, most of which involve mixed metal atoms and/or partially occupied oxygen sites: 2.20 Å for $BaGd_2Mn_2O_7$ [33], 2.197 Å for $Ba_{0.5}Bi_{1.5}O_{2.16}$ [34], and 1.980 Å for $Bi_{1.5}Ba_{0.25}LaCu_2O_{8.25}$ [35].

3.5. Polyhedra arrangement

Fig. 8 shows a slab of (0 0 1) plane around $z = 0$ with a thickness of ~5 Å. Slabs at different heights such as $z = 1/4$, 1/2, or 3/4 have the same environment, but with translation in the *ab*-plane or at 90° orientations. While $W^{(1)}O_6$ octahedra are isolated from each other by Ba1 and Ba2 atoms, the $W^{(2)}O_{18/3}$ polyhedra arrangement along the [110] direction passing through the origin in Fig. 8 displays 1-D arrangement without blocking atoms. Each W2 has six nearest W2 atoms in the 3D network of the crystal structure, thus three linear $W^{(2)}O_{18/3}$ polyhedra arrangements are passing through W2 in the direction along [110], [101] and [011].

The metal vacancies, indicated as V_u and V_d in Fig. 8, lie at the 8*a* ($\frac{1}{8}$, $\frac{1}{8}$, $\frac{1}{8}$) site, and are located at the top (at $z = \frac{1}{8}$) and bottom (at $z = -\frac{1}{8}$) of the slab, respectively. It should be noted that the vacancies lie in between two adjoining $W^{(2)}O_{18/3}$ polyhedra. In three dimensions, the vacancies are in the center of the tetrahedron formed by the four nearest $W^{(2)}O_{18/3}$ polyhedra. The O2 ions of the $W^{(2)}O_{18/3}$ polyhedron are directed to the neighboring $W^{(2)}O_{18/3}$ polyhedra. The closest inter-polyhedral O–O contact is O2–O2 with a distance of 2.05 Å, too close to be occupied simultaneously, as indicated by the partial occupancy of less than one half. Ba2 bridges such inter-polyhedral O2 ions with *d*(Ba2–O2) of 2.727 Å, and an (O2–Ba2–O2) angle of 49.0°. The other oxygen O3 bridges the two nearest Ba2 ions with a distance of 2.592 Å and a (Ba2–O3–Ba2) angle of 113.6°.

3.6. Bond-valence summations (BVS)

The empirical expression for bond valence, which has been widely adopted to estimate valences in inorganic solids, was used to check the $Ba_{11}W_4O_{23}$ crystal structure. The bond-valence sums [36] calculated with the program Bond_Str [37] for Ba1, Ba2, Ba3, W1, W2, O1, O2, O3, and O4 are 1.52, 2.23, 2.51, 5.78, 5.56, 1.99, 1.91, 2.07, and 2.74 v.u., respectively. These match the expected charges of the ions reasonably. The lower valence sum for Ba1 resulted from the longer Ba1–O1 bond distances (3.050 Å). The higher sums for Ba3 and O4 resulted mainly from the short Ba3–O4 distance (2.13 Å).

3.7. Crystal structure at 1100 °C

Rietveld refinement (Fig. 4; Table 6) and Fourier map analysis for the *in situ* high-temperature X-ray data for $Ba_{11}W_4O_{23}$ at 1100 °C showed that the structure is basically isostructural to the quenched structure. Electron densities surrounding W1 and W2 at high temperature were almost identical to those observed for the quenched phase at room temperature. Because neutron diffraction data at 1100 °C were not available, positional parameters and occupancies for O2, O3 and O4 could not be refined sufficiently using X-ray data alone. Instead, these parameters were adopted from the quenched phase data and fixed in the Rietveld refinement. The unit cell increases by 1.8% from room temperature (17.1823 Å) to 1100 °C (17.4966 Å). As expected, all the thermal parameters at high temperature are much larger than those at RT.

4. Conclusions

The important contribution of the present study is the discovery of a new type of perovskite-related superstructure with *A*-site metal-vacancy ordering, disordered oxygens and anionic vacancies. Since the structure–property relationship is important for many applications, it is expected that substitution at the Ba, W, and/or oxygen sites with the present chemical formula or a small variation thereof would produce new materials with novel properties of interest.

Acknowledgments

The author thanks Prof. A.W. Sleight at Oregon State University for kind advice and encouragement, Prof. B.J. Wuensch at M.I.T. for helpful discussion, and Dr. K.-P. Hong and Dr. Y.N. Choi at KAERI for assistance with neutron scattering measurements.

References

[1] R.H. Mitchell, Perovskites: Modern and Ancient, Almaz Press, Inc., Thunder Bay, Ont., 2002.
[2] M.T. Anderson, K.B. Greenwood, G.A. Taylor, K.R. Poeppelmeier, Prog. Solid State Chem. 22 (1993) 197–233.
[3] A. Varez, Y. Inaguma, M.T. Fernandez-Diaz, J.A. Alonso, J. Sanz, Chem. Mater. 15 (2003) 4637–4641.
[4] P.D. Battle, J.E. Bennett, J. Sloan, R.J.D. Tilley, J.F. Vente, J. Solid State Chem. 149 (2000) 360–369.
[5] M. Wakeshima, Y. Hinatsu, Solid State Commun. 136 (2005) 499–503.
[6] K.G. Bramnik, G. Miehe, H. Ehrenberg, H. Fuess, A.M. Abakumov, R.V. Shpanchenko, V.Yu. Pomjakushin, A.M. Balagurov, J. Solid State Chem. 149 (2000) 49–55.
[7] D.D. Khalyavin, A.M.R. Senos, P.Q. Mantas, J. Phys.: Condens. Matter 17 (2005) 2585–2595.

[8] U. Treiber, S. Kemmler-Sack, Z. Anorg. Allg. Chem. 463 (1980) 132–136.
[9] D.J.W. Ijdo, R.B. Helmholdt, Acta Crystallogr. C 49 (1993) 652–654.
[10] U. Treiber, S. Kemmler-Sack, Z. Anorg. Allg. Chem. 470 (1980) 103–108.
[11] M.T. Anderson, J.T. Vaughey, K.R. Poeppelmeier, Chem. Mater. 5 (1993) 151–165.
[12] T.I. Bylichkina, L.I. Soleva, E.A. Pobedimskaya, M.A. Porai-Koshits, N.V. Belov, Kristallografiya 15 (1970) 165–167.
[13] S. Kemmler-Sack, U. Treiber, Z. Anorg. Allg. Chem. 455 (1979) 65–68.
[14] L.M. Kovba, L.N. Lykova, V.L. Balashov, A.L. Kharlanov, Koor. Khim. 11 (1985) 1426–1429.
[15] H.P. Rooksby, E.G. Steward, Nature 157 (1946) 548–549.
[16] E.G. Steward, H.P. Rooksby, Acta Crystallogr. 4 (1951) 503–507.
[17] L.L.Y. Chang, M.G. Scroger, B. Phillips, J. Am. Ceram. Soc. 49 (1966) 385–390.
[18] L.M. Kovba, L.N. Lykova, N.N. Shevchenko, Russ. J. Inorg. Chem. 16 (1971) 1150–1152.
[19] E.R. Kreidler, J. Am. Ceram. Soc. 55 (1972) 514–519.
[20] NBS Monograph 25 (19) (1982) 21–22.
[21] V.L. Balashov, A.A. Kharlanov, O.I. Kondratov, V.V. Fomichev, Russ. J. Inorg. Chem. 36 (1991) 254–257.
[22] G.M. Sheldrick, SHELXS-86, Universität Göttingen, Germany, 1986.
[23] P.W. Betteridge, J.R. Carruthers, R.I. Cooper, C.K. Prout, D.J. Watkin, J. Appl. Cryst. 36 (2003) 1487.
[24] A.C. Larson, R.B. Von Dreele, General structure analysis system, Report No. LA-UR-86-748, Los Alamos National Laboratory, Los Alamos, NM, 1987.
[25] B. Betz, H.J. Schttenhelm, S. Kemmler-Sack, Z. Anorg. Allg. Chem. 484 (1982) 177–186.
[26] U. Treiber, A.J. Griffiths, S. Kemmler-Sack, Z. Anorg. Allg. Chem. 473 (1981) 171–177.
[27] S. Kemmler-Sack, I. Jooss, Z. Anorg. Allg. Chem. 440 (1978) 203–209.
[28] G. Baldinozzi, P. Sciau, J. Lapasset, Phys. Status Solidi A 133 (1992) 17–23.
[29] G. Baldinozzi, P. Sciau, P. Pinot, D. Grebille, Acta Crystallogr. B 51 (1995) 668–673.
[30] P.D. Battle, C.R.A. Catlow, J. Drennan, A.D. Murray, J. Phys. Chem. 16 (1983) 561–566.
[31] B.J. Wuensch, Mater. Sci. Eng. B 18 (1993) 186–200.
[32] R.D. Shannon, Acta Crystallogr. A 32 (1976) 751–767.
[33] N. Kamegashira, H. Satoh, T. Mikami, J. Alloys Compd. 311 (2000) 69–73.
[34] S. Esmaeilzadeh, P. Berastegui, J. Grins, H. Rundlöf, J. Solid State Chem. 152 (2000) 435–440.
[35] C. Michel, D. Pelloquin, M. Hervieu, B. Raveau, J. Solid State Chem. 112 (1994) 362–366.
[36] I.D. Brown, D. Altermatt, Acta Crystallogr. B 41 (1985) 244–247.
[37] J. Rodriguez-Carvajal, *Bond_Str* (ver. March 2005), France, Laboratorie Leon Brillouin, CEA-Saclay, 2005.